ACS APPLIED MATERIALS & INTERFACES

Research Article

Cite This: ACS Appl. Mater. Interfaces 2018, 10, 39745−39756

www.acsami.org

Microstructure Determines Water and Salt Permeation in Commercial Ion-Exchange Membranes

R. S. Kingsbury, S. Zhu, S. Flotron, and O. Coronell*

Department of Environmental Sciences and Engineering, Gillings School of Global Public Health, The University of North Carolina at Chapel Hill, Chapel Hill, North Carolina 27599, United States

Supporting Information

ABSTRACT: Ion-exchange membrane (IEM) performance in electrochemical processes such as fuel cells, redox flow batteries, or reverse electrodialysis (RED) is typically quantified through membrane selectivity and conductivity, which together determine the energy efficiency. However, water and co-ion transport (i.e., osmosis and salt diffusion/fuel crossover) also impact energy efficiency by allowing uncontrolled mixing of the electrolyte solutions to occur. For example, in RED with hypersaline water sources, uncontrolled mixing consumes 20−50% of the available mixing energy. Thus, in addition to high selectivity and high conductivity, it is desirable for IEMs to have low permeability to water and salt to minimize energy losses. Unfortunately, there is very little quantitative water and salt permeability information available for commercial IEMs, making it difficult to select the best membrane for a particular application. Accordingly, we measured the water and salt transport properties of 20 commercial IEMs and analyzed the relationships between permeability, diffusion, and partitioning according to the solution-diffusion model. We found that water and salt permeance vary over several orders of magnitude among commercial IEMs, making some membranes better suited than others to electrochemical processes that involve high salt concentrations and/or concentration gradients. Water and salt diffusion coefficients were found to be the principal factors contributing to the differences in permeance among commercial IEMs. We also observed that water and salt permeability were highly correlated to one another for all IEMs studied, regardless of polymer type or reinforcement. This finding suggests that transport of mobile salt in IEMs is governed by the microstructure of the membrane and provides clear evidence that mobile salt does not interact strongly with polymer chains in highly swollen IEMs.

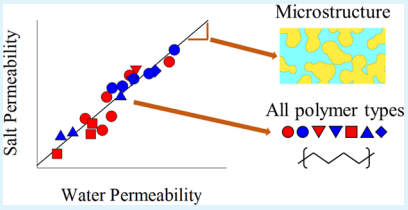

KEYWORDS: *Ion exchange membrane, diffusion, osmosis, permeability, solution-diffusion model*

1. INTRODUCTION

Ion-exchange membranes (IEMs) are versatile materials used in a variety of electrochemical processes for water and waste treatment, energy production, energy storage, and industrial separation.[1−3] IEM performance in electrochemical systems is typically quantified through membrane permselectivity and resistance, which together determine the energy efficiency and/or power output of a given process.[4−6] Permselectivity measures the degree to which IEMs selectively allow ions of opposite charge (counter-ions) to permeate, while excluding ions of like charge (co-ions).[7] In a cation-exchange membrane (CEM), for example, cations are the counter-ions and anions are the co-ions.

Permselectivity and resistance concern the transport of counter-ions. However, water and co-ions also permeate through IEMs (see Figure 1).[8−15] Water permeates the membrane by two mechanisms: osmosis and electroosmosis. Osmosis is simply the diffusion of water, whereas electro-osmosis refers to the transport of water molecules in the hydration shells of counter-ions permeating the IEM as a result of migration in an electric field. Co-ions permeate IEMs accompanied by counter-ions as "mobile salt."[10,16] In dense polymers in which water permeation by convection is negligible, co-ion transport can be viewed as salt diffusifon through the membrane.[10,17]

Because neither osmosis nor salt diffusion responds to electric fields, both have a detrimental effect on the energy or separation efficiency of electrochemical processes such as electrodialysis (ED) and reverse electrodialysis (RED).[12,13,18−20] Osmosis and salt diffusion both lower the salt concentration in the concentrated feed, which in ED compromises separation and in RED causes uncontrolled mixing (i.e., mixing that does not produce electricity, Figure 1). The magnitude of the effects of water and salt transport on efficiency depends on both the process (ED, RED, energy storage, etc.) and the process conditions (e.g., salt concentrations). For example, in RED with seawater and river water, the combined effects of salt diffusion and osmosis reduce power output by approximately 10−25%.[11,12,18] Another study found that uncontrolled mixing reduced the current efficiency of RED from 65% to only 20%.[13] With larger concentration gradients (e.g., hypersaline water sources or industrial brines), uncontrolled mixing reduces the current efficiency by 20−

Received: August 22, 2018
Accepted: October 25, 2018
Published: October 25, 2018

DOI: 10.1021/acsami.8b14494
ACS Appl. Mater. Interfaces 2018, 10, 39745−39756

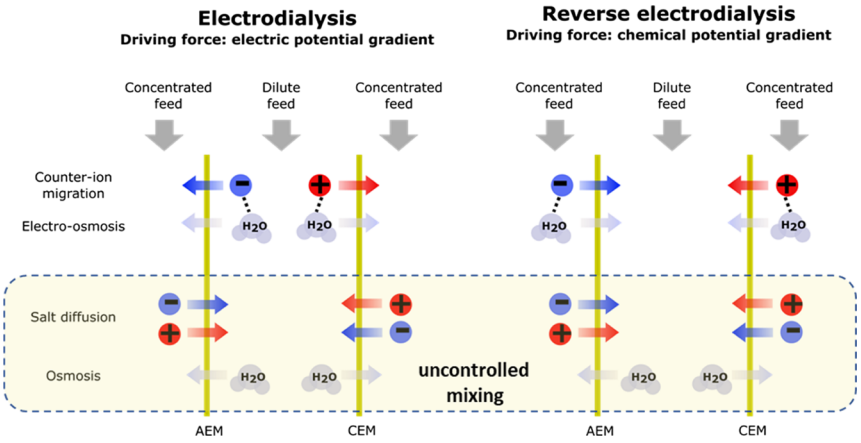

Figure 1. Mass transport phenomena occurring inside electrodialysis (ED) (left) and reverse electrodialysis (RED) (right) stacks. Salt diffusion and osmosis do not respond to electric fields and thus constitute "uncontrolled mixing" of the respective feed solutions.

50%.[18] In ED desalination, osmosis reduced the current efficiency by approximately 10% compared to ideally selective membranes,[13] and salt diffusion was estimated to increase the required energy consumption by 2−3 times.[19] In energy storage applications, osmosis reduces the round-trip energy efficiency by as much as 50%, while salt diffusion has a similar or smaller impact, depending on the membrane used.[14,15,21,22] The effect of osmosis on energy efficiency increases dramatically with higher salt concentrations, limiting the concentrations that can be used and consequently restricting the energy density of these systems.[22]

Thus, in addition to high permselectivity and low resistance, it is desirable for IEMs to have low permeability to water and salt to minimize energy losses in electrically driven processes. Conversely, in diffusion-driven processes (e.g., diffusion dialysis), higher permeability may be desired.[23] Unfortunately, very little quantitative data exist for the water and salt permeance of commercial IEMs. Isolated reports in the literature place the water permeance of some commercial IEMs in the range 0.005−0.17 L m^{-2} h^{-1} bar^{-1},[13,22−24] and one study[20] reported the salt permeance in the 0.003−0.025 L m^{-2} h^{-1} range for lab-prepared IEMs based on commercial polymer solutions. Another study reported diffusion coefficients and thicknesses for a set of commercial IEMs, from which it is possible to calculate the permeance if the experimental conditions are known.[11] However, there has been no systematic measurement of water and salt permeance for a large set of commercial membranes under consistent experimental conditions, making it difficult to compare IEMs and select the best for a particular application. Furthermore, it is currently unknown how water and salt permeance are related to other membrane properties. Such knowledge is necessary for the development of advanced IEMs.

Accordingly, the objectives of this study were to (1) quantify the water and salt transport characteristics of commercially available IEMs; (2) evaluate whether water and salt transport are controlled by the thickness or the intrinsic transport properties (i.e., partitioning and/or diffusion) of the membranes; and (3) examine relationships between these transport characteristics and membrane polymer type. We measured the water and salt permeability of 20 IEMs using a two-compartment cell and characterized other properties using well-known techniques. Using the solution-diffusion model framework, we report partition and diffusion coefficients for both water and salt for each membrane and relate the permeability, partition, and diffusion coefficients to the polymer backbone type. Our results show that membrane microstructure is the primary factor governing water and salt transport in IEMs.

2. THEORETICAL BACKGROUND

2.1. Solution-Diffusion Model. The solution-diffusion model is the most widely accepted framework for describing the transport of small molecules, such as water and salt, through dense polymer membranes.[8,10,17] In this model, molecules are assumed to permeate the membrane by partitioning from the bulk solution into the membrane polymer at the upstream interface, diffusing through the membrane, and then partitioning into the bulk solution at the downstream interface. As such, the solvent and solute permeate independently of one another (i.e., convection and frictional coupling of fluxes are neglected). Although there is not a vast body of literature confirming whether the solution-diffusion model is rigorously applicable to IEMs, its validity is well established for desalination polymers,[10] and IEMs have pore sizes in the same size range as reverse osmosis (RO) and nanofiltration (NF) membranes (0.4−2 nm for RO/NF membranes vs 0.4−1.5 nm for IEMs).[2,13,26−28] Furthermore, several researchers have applied the solution-diffusion model to describe salt transport in IEMs with good results. Therefore, we adopted the solution-diffusion model to analyze water and salt transport data throughout this paper.

The permeability P (m^2 s^{-1}) represents the steady-state flux of a molecule through the membrane, normalized by membrane thickness and the driving force.[8] Permeability is the product of a kinetic parameter—the molecular diffusion coefficient D (m^2 s^{-1})—and a thermodynamic parameter—the molecular partition coefficient K (dimensionless). Thus

$$P = DK \tag{1}$$

The diffusion coefficient is a measure of how quickly the substance transports through the membrane, while the partition coefficient is defined as the concentration of the substance in the membrane divided by its concentration in bulk solution. Throughout this manuscript, we will use subscripts w and s to denote transport properties for water and salt, respectively.

2.2. Donnan−Manning Theory. Kamcev et al. recently showed that Manning's counter-ion condensation theory can

DOI: 10.1021/acsami.8b14494
ACS Appl. Mater. Interfaces 2018, 10, 39745−39756

Table 1. Structural, Chemical, and Physical Properties of IEMs Used in This Work[a]

membrane	polymer type[b]	reinforcement[b]	thickness[c], μm	IEC[d], mequiv g^{-1}	SD[e], g H_2O g^{-1}	C_{fix}[f], mol L^{-1}	Manning parameter[g]	notes
Anion Exchange Membranes								
Selemion AMV	St/DVB	PVC	109 ± 3	2.02 ± 0.04	0.19 ± <0.01	10.9 ± 0.3	1.6 ± 0.3	
Selemion ASA	St/DVB	PVC	96 ± 3	2.13 ± 0.04	0.16 ± <0.01	13.4 ± 0.3	1.1 ± 0.1	monovalent-selective
Selemion ASV	St/DVB	PVC	121 ± 5	2.02 ± 0.02	0.19 ± <0.01	10.6 ± 0.2	1.0 ± <0.1	monovalent-selective
Neosepta ACS	St/DVB	PVC	117 ± 3	1.97 ± 0.01	0.24 ± 0.01	8.2 ± 0.3	1.3 ± 0.1	monovalent-selective
Neosepta AMX	St/DVB	PVC	133 ± 1	1.42 ± 0.03	0.16 ± 0.01	9.0 ± 0.5	1.0 ± 0.1	
Fumasep FAS-15	pAro	none	20 ± 3	1.77 ± 0.03	0.10 ± 0.01	18.1 ± 1.8	2.2 ± 0.5	
Fumasep FAS-30	pAro	none	30 ± 1	2.15 ± 0.09	0.12 ± 0.01	17.3 ± 1.3	1.4 ± 0.1	
Fumasep FAB-30	pAro	none	24 ± 1	1.35 ± 0.06	0.09 ± 0.01	14.5 ± 1.1	1.2 ± 0.2	low-IEC, low water transfer
PCCell PC-SA	St/DVB	polyester	232 ± 3	1.69 ± 0.06	0.29 ± 0.01	5.9 ± 0.3	3.1 ± 0.4	
Fujifilm type III AEM	MAm	PE/PP	103 ± 3	1.52 ± 0.02	0.35 ± 0.01	4.4 ± 0.1	0.8 ± <0.1	
Cation Exchange Membranes								
Selemion CMV	St/DVB	PVC	105 ± 2	1.89 ± 0.09	0.23 ± 0.01	8.3 ± 0.5	1.5 ± 0.1	
Selemion CSO	St/DVB	PVC	97 ± 2	2.20 ± 0.02	0.25 ± <0.01	8.6 ± 0.1	1.5 ± 0.1	
Neosepta CMS	St/DVB	PVC	136 ± 3	2.28 ± 0.05	0.28 ± 0.01	8.2 ± 0.4	1.6 ± 0.1	monovalent-selective
Neosepta CMX	St/DVB	PVC	170 ± 4	1.77 ± 0.01	0.22 ± 0.01	7.9 ± 0.3	1.3 ± 0.1	
Fumasep FKE-15	sPEEK	none	20 ± 1	1.48 ± 0.04	0.11 ± 0.02	13.5 ± 2.1	3.0 ± 0.4	
Fumasep FKE-30	sPEEK	none	32 ± 1	1.52 ± 0.02	0.13 ± 0.01	12.1 ± 0.9	1.1 ± 0.1	
Fumasep FKL-30	sPEEK	none	26 ± 2	1.10 ± 0.03	0.09 ± 0.01	11.9 ± 1.2	2.1 ± 0.3	low-IEC, low water transfer
PCCell PC-SK	St/DVB	polyester	98 ± 3	1.25 ± 0.04	0.37 ± 0.01	3.4 ± 0.1	1.7 ± 0.1	
Nafion N115	PFSA	none	126 ± 4	0.92 ± 0.01	0.11 ± <0.01	8.6 ± 0.3	1.1 ± 0.1	
Fujifilm type III CEM	MAm	PE/PP	119 ± <1	1.96 ± 0.03	0.38 ± 0.01	5.1 ± 0.1	1.5 ± <0.1	

[a]Reported values represent the average and propagated standard error of at least three replicates. [b]MAm = methacrylamide, pAro = polyaromatic, St/DVB = styrene−divinylbenzene copolymer, sPEEK = sulfonated poly(etheretherketone), PFSA = perfluorinated sulfonic acid, PE = poly(ethylene), PP = poly(propylene), and PVC = poly(vinylchloride). Structural details that are not available in literature were obtained by personal communication with the respective manufacturers. Structural and reinforcement details for the Fujifilm membranes are assumed based on information in the patent literature.[32,33] [c]Wet thickness measured after experiments in contact with 4 M NaCl (concentrated side) and pure water (dilute side) (see Section 3.2). [d]Ion-exchange capacity (IEC; see Section 3.4). A comparison with the literature and manufacturer-reported IEC values is provided in Section S9. [e]Swelling degree (SD) of the membrane in the NaCl form in equilibrium with 4 M NaCl (see Section 3.3). [f]Fixed charge density per unit of water sorbed by the membrane (see Section 3.4). [g]Calculated from measured co-ion partition coefficient in 0.5 M NaCl (see Section 3.5 and Table S2).

be used in conjunction with Donnan theory to predict salt partition coefficients (K_s) in IEMs with good accuracy.[9,29,30] The crucial parameter in Manning theory is the Manning parameter, ξ, which is defined as

$$\xi = \frac{\lambda_b}{b} \tag{2}$$

where b (m) is the distance between fixed charge sites along the polymer chain and λ_b (m) is the Bjerrum length of the solution inside the membrane. If ξ and the fixed charge concentration of an IEM are known, Donnan−Manning theory can be used to calculate the mobile salt concentration inside the membrane as a function of bulk salt concentration.[29] Conversely, ξ can be determined from experimental data if the concentration of fixed charges and mobile salt in an IEM are known. Given the very recent emergence of Donnan−Manning theory as a useful tool for predicting IEM behavior, ξ has only been reported for three commercial IEMs to date.[29]

3. EXPERIMENTAL SECTION

3.1. Ion-Exchange Membranes. We measured the properties of 20 homogeneous commercial IEMs with a diverse range of characteristics representative of a majority of the IEMs commonly studied in the literature. Table 1 summarizes the structural, physical, and chemical characteristics of the IEMs studied. All membranes were stored as directed by the respective manufacturers. Prior to measurements, membrane coupons were immersed in sodium chloride solutions at room temperature for a minimum of 24 h. The concentration of the equilibration solution was matched to that of the measurement solution, and the solution was changed at least three times to ensure complete conversion of the functional groups to either Na^+ or Cl^- form. We prepared all solutions from reagent grade sodium chloride (Alfa Aesar, 99+% purity). All measurements reported in this work represent the mean and standard error of at least three independent measurements of replicate membrane coupons.

Note that we tested a mixture of reinforced and nonreinforced membranes. In reinforced membranes, the active (charged) polymer fills the voids in a hydrophobic backing fabric that is generally considered not to absorb any water.[30] The presence of the backing creates a composite structure so that the properties of the membrane (e.g., swelling, permeability, partition coefficients, etc.) do not represent those of the active polymer, but rather of the composite.[30,31] In general, it is possible to correct for the presence of the backing fabric if its geometry is known,[31] but we were unable to obtain the necessary information to do so in this study because of the proprietary nature of commercial IEMs. Therefore, all properties reported herein are those of the whole membrane, including the reinforcing fabric (where applicable). Based on a sensitivity analysis we performed (see Supporting Information) and the fact that we obtained similar values of permeability, partition, and diffusion coefficients for reinforced and nonreinforced membranes, we conclude the effect of the reinforcing fabric on the transport properties we present in our work to be small.

DOI: 10.1021/acsami.8b14494
ACS Appl. Mater. Interfaces 2018, 10, 39745−39756

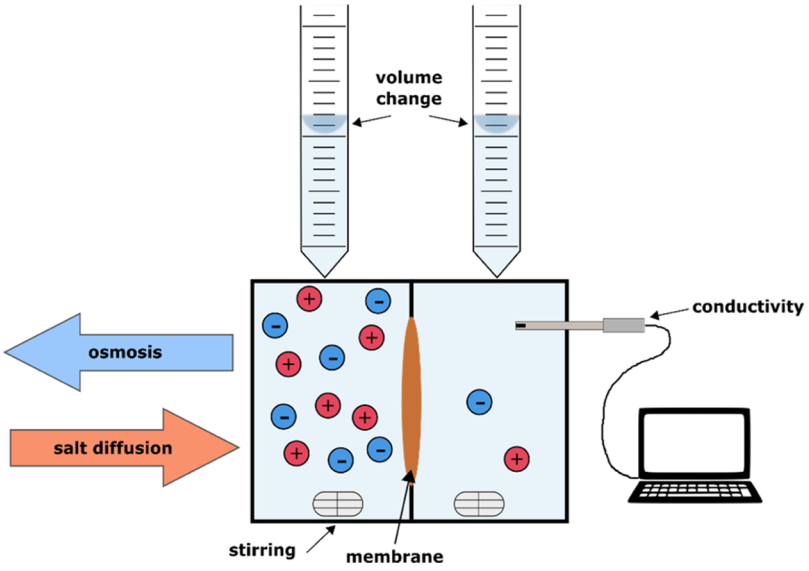

Figure 2. Schematic of a two-compartment cell used for permeability measurements. Compartment volume = 16 mL, exposed membrane area = 7.55 cm^2, stirring rate = 300 rpm. Burets with 0.05 mL graduations were connected to each compartment through small openings (diameter <1 mm) and approximately 15 cm of tubing. At the beginning of each experiment, the fluid levels in the two burets were equalized to prevent any hydrostatic pressure difference between the compartments.

3.2. Membrane Thickness. We measured the membrane thickness with a micrometer (L.S. Starrett Co., Athol, MA, model 3732XFL-1) immediately following tests of osmosis and diffusion (see Section 3.6). After removing the membrane coupon from the test cell, we blotted it dry with a laboratory wipe and measured its thickness. It is important to measure the thickness in this way because the membrane may swell differently when exposed to a concentration gradient different from that between pure water and 4 M NaCl solution.

3.3. Water Content. The swelling degree (SD) of IEMs was measured gravimetrically.[4] Membrane coupons were equilibrated in the desired concentration of salt solution as described in Section 3.1, then blotted dry with a laboratory wipe,[34,35] and weighed immediately on an analytical balance. The membranes were subsequently dried in an incubator at 65 °C for 48 h[36] and then weighed again. The SD (g H_2O per g dry polymer) was calculated as[4]

$$\mathrm{SD} = \frac{m_{\mathrm{wet}} - m_{\mathrm{dry}}}{m_{\mathrm{dry}}} \tag{3}$$

where m_{wet} (g) and m_{dry} (g) are the wet and dry masses, respectively. Membrane coupons were not used for any further analysis after drying.[34,35]

We used the SD to calculate the volume fraction of water in the membrane, φ_w, and the water partition coefficient, K_w, as[10]

$$\varphi_w = \frac{\mathrm{SD}}{\mathrm{SD} + \frac{\rho_w}{\rho_p}} \tag{4}$$

and

$$K_w = \frac{\varphi_w M_w}{C_w^s V_w} \tag{5}$$

where ρ_p (g mL^{-1}) is the dry polymer density, for which we used a value of 1.15 g mL^{-1} based on a weighted average of the dry densities of the base polymers for the IEMs used in this work[37−41] (see Table 1). M_w (18.015 g mol^{-1}) is the molar mass of water, and C_w^s (g L^{-1}) is the mass concentration of water in the bulk solution. Note that when C_w^s is approximately equal to the density of pure water, which is true within ~1% for salt concentrations lower than 0.5 M, then, $K_w \approx \varphi_w$. Although the two parameters are effectively equal in much of the desalination literature,[10,42] we will make a distinction between them because of the high salt concentration used in this work (4 M, C_w^s = 915.5 g L^{-1}). Throughout the text, we use the terms "water sorption," "water uptake," or "swelling" to refer generally to water absorption by IEMs as indicated by φ_w, SD, or K_w.

3.4. Membrane Charge. We quantified membrane charge through ion exchange capacity (IEC, mequiv charge per g dry polymer) and fixed charge concentration (mol charge per L of water absorbed by the membrane). IEC was determined according to well-established titration methods. For CEMs, we soaked membrane coupons in 1 M HCl for at least 12 h[4] to convert charged sites to H^+ form, replacing the solution at least twice[43,44] to ensure complete ion exchange. The membranes were then removed from the solution, rinsed thoroughly with deionized (DI) water, and immersed in 2 M NaCl for at least 3 h, again changing the solution at least twice.[4] We collected all of the discarded NaCl solution and analyzed it for H^+ by titration with 0.1 M NaOH.[36] For anion-exchange membranes (AEMs), we soaked the membrane coupons in 2 M NaCl for at least 12 h, changing the solution at least twice, to convert all charged sites to Cl^- form. Then, we quickly removed the membranes and rinsed with DI water that had been degassed under nitrogen. Degassing is necessary to prevent dissolved CO_2 from exchanging with Cl^- ions and biasing the measurement.[43] The membranes were then placed in 2 M $NaNO_3$ solution for at least 6 h,[36] during which the solution was changed at least twice. The exchanged solutions were collected and analyzed for the Cl^- ion by titration with 0.1 M $AgNO_3$.[4,36] Both AEMs and CEMs were subsequently dried in an incubator at 65 °C for 48 h.[36] IEC was calculated as[4]

$$\mathrm{IEC} = \frac{V_{\mathrm{titrant}} C_{\mathrm{titrant}}}{m_{\mathrm{dry}}} \tag{6}$$

where V_{titrant} (L) and C_{titrant} (M) are the volume and concentration of the titrant used, respectively, and m_{dry} (g) is the dry weight of the membrane coupon.

The concentration of fixed charges inside the IEM, C_{fix}, in units of equivalents of charge per L of water absorbed by the membrane, is given by

$$C_{\mathrm{fix}} = \frac{\mathrm{IEC}}{\mathrm{SD}} \rho_w \tag{7}$$

3.5. Co-Ion Sorption and Manning Parameter. Kamcev et al.[29] showed that salt sorption data obtained at a single salt concentration can be used to calibrate the Manning parameter ξ and predict salt sorption at any other salt concentration. Accordingly,

DOI: 10.1021/acsami.8b14494
ACS Appl. Mater. Interfaces 2018, 10, 39745−39756

we used procedures similar to those of Kamcev et al.[29,30] to determine mobile salt sorption and ξ in 0.5 M NaCl and then calculated the concentration of mobile salt in each membrane in 4 M NaCl. Briefly, we equilibrated the membrane coupons in 0.5 M NaCl as described in Section 3.1. We then removed each coupon from solution, blotted the surface dry with a laboratory wipe, weighed it, and placed it in a plastic vial containing 30 mL of pure water for at least 48 h. The mobile salt in the membrane desorbed into the water during this period. Kamcev et al. showed that a single desorption step (e.g., without changing the water) was sufficient to effectively desorb all mobile salt in the membrane.[45] After desorption, we analyzed the co-ion concentration (Na^+ for AEMs, Cl^- for CEMs) using inductively coupled mass spectrometry for Na^+ (see Supporting Information for method details) and an ion-selective electrode (Fisher Scientific, Fair Lawn, NJ, model 13-620-100) for Cl^-. The membrane coupons were removed from the vials, dried in an incubator at 65 °C for 48 h,[36] and weighed. The co-ion concentration in the desorption solution and the membrane weights were used to obtain the co-ion concentration in the membrane ($\bar{C}_s$, mol per unit volume of water sorbed) as

$$\bar{C}_s = \frac{C_c V_w \rho_w}{m_{wet} - m_{dry}} \tag{8}$$

where C_c (M) is the co-ion concentration in the desorption solution, V_w (30 mL) is the volume of the desorption solution, ρ_w (0.998 g mL^{-1}) is the density of water, and m_{wet} and m_{dry} (g) are the wet and dry masses of the membrane coupon, respectively. The measured co-ion concentrations in 0.5 M NaCl, the measured Manning parameters, and the calculated co-ion concentrations in 4 M NaCl are given in Table S2.

Next, K_s was calculated as

$$K_s = \frac{\bar{C}_s \varphi_w}{C_s} \tag{9}$$

where $\bar{C}_s$ (see Section 3.5) and C_s are the (mobile) salt concentrations inside the IEM and in bulk solution, respectively. Throughout the text, membrane-phase salt concentrations are reported in units of mol salt per L of water absorbed by the membrane, as required by Manning theory.[9,29,30] φ_w in eq 9 serves as a conversion factor to convert the numerator into units of mol salt per L of swollen polymer, which is the appropriate unit of measure to use when calculating K_s.[9]

3.6. Simultaneous Measurement of Osmosis and Diffusion through IEMs. We measured water and salt permeability simultaneously using the two-compartment cell illustrated in Figure 2. One side of the cell contained 4 M NaCl solution and the other contained pure water. We chose 4 M NaCl for the concentrated solution to maximize the rate of osmosis and facilitate water transport measurements (as suggested by Tanaka[36]) and also because nonideal transport of water and salt is of greatest concern in IEM processes involving high concentrations.[18] Membrane coupons were stabilized in the cell for 1−4 h prior to measurements to allow for osmosis and diffusion to reach a pseudo-steady state. The solutions were changed at least once during the stabilization period, and the compartments were refilled with fresh solutions immediately prior to the measurement. Once measurements began, the salt solutions in both compartments were stirred at 300 rpm by means of magnetic stir bars.

During measurement of salt and water permeability, water flowed into the high-concentration compartment as a result of osmosis, while salt diffused into the pure water compartment. Each cell compartment was sealed and connected to a buret with 0.05 mL markings, allowing the volume change in the compartment to be measured with high precision. We measured changes in the volumes of the compartments and in the salt concentration in the dilute compartment with time for at least 60 min or until the volume change was at least 0.25 mL (corresponding to 5 markings on the buret). To obtain precise volume measurements, we watched the meniscus in each buret and waited until it exactly crossed each marking and then recorded both the volume and the elapsed time, rather than recording volume at predetermined time intervals. Water flux was obtained from the rate of volume change and used to calculate water permeance and permeability (see Section 3.7).

A conductivity probe (eDAQ Pty Ltd, Sydney, Australia, model ET915) was placed in the pure water compartment to quantify the change in conductivity with time. A calibration curve was used to obtain salt concentration from conductivity measurements, and the time series of salt concentration data was used to calculate the salt permeance and permeability (see Section 3.8).

3.7. Calculation of Water Permeance and Permeability. Because we measured osmosis (water flux) and diffusion simultaneously, it was necessary to account for the diluting effect of osmosis on the salt concentration gradient. In other words, over time, water flux from the pure water compartment diluted the salt concentration in the other compartment, lowering the driving force for diffusion and osmosis. We accounted for this effect by solving an appropriate mass balance (see Supporting Information).

First, water permeance A (L m^{-2} h^{-1} bar^{-1}) was calculated from the steady-state volumetric water flux n_w (L m^{-2} h^{-1}) as[10]

$$A = \frac{n_w}{\Delta P - \Delta\pi} \tag{10}$$

where ΔP and $\Delta\pi$ (bar) are the net differences in hydrostatic and osmotic pressure, respectively, across the membrane. In our experiments, both burets were filled to the same initial height, so $\Delta P = 0$, while $\Delta\pi = 243.4$ bar (calculated using the Gibbs equation and the Pitzer model[46−48] for activity coefficients).

Next, we calculated D_w from water permeance as[10,42]

$$D_w = \frac{AL}{\varphi_w}\frac{RT}{V_w}(1-\varphi_w)^2(1-2\chi\varphi_w) \tag{11}$$

where R (8.314 J mol^{-1} K^{-1}) is the ideal gas constant, T (K) is the temperature, L (m) is the swollen membrane thickness (Section 3.2), V_w (0.0182 L mol^{-1}) is the molar volume of water, φ_w (dimensionless) is the volume fraction of water in the membrane (Section 3.3), and χ (dimensionless) is the Flory−Huggins interaction parameter, determined by fitting water sorption data in 4 M NaCl to the Flory−Huggins model (eq S15). In highly swollen polymers such as many of the IEMs we studied, convective frame-of-reference and thermodynamic effects must be accounted for when converting water permeance into water permeability.[10,42] Eq 11 reflects both corrections (see Supporting Information for detailed discussion).

Water permeability, P_w, was obtained from the water diffusion coefficient D_w and the water partition coefficient K_w according to

$$P_w = D_w K_w \tag{12}$$

3.8. Calculation of Salt Permeance and Permeability. Similar to water, we analyzed salt diffusion data to obtain salt permeability, diffusion, and partition coefficients (P_s, D_s, and K_s, respectively) according to

$$P_s = D_s K_s \tag{13}$$

P_s was calculated directly from the observed salt concentration versus time data using a mass balance that accounted for the effects of both osmosis and diffusion on the salt concentration in the dilute compartment of the cell (see Supporting Information).

Having obtained K_s (Section 3.5), we then calculated the salt diffusion coefficient D_s as

$$D_s = \frac{P_s}{K_s} \tag{14}$$

Finally, the salt permeance B (L m^{-2} h^{-1}) was obtained from the measured salt permeability and thickness as

$$B = \frac{P_s}{L} \tag{15}$$

DOI: 10.1021/acsami.8b14494
ACS Appl. Mater. Interfaces 2018, 10, 39745−39756

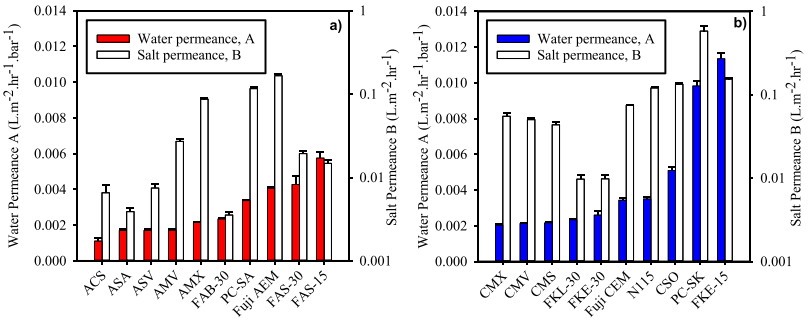

Figure 3. Water permeance (solid bars, linear scale) and salt permeance (empty bars, log scale) of commercial (a) AEMs and (b) CEMs measured in a diffusion cell containing 4 M NaCl and pure water. In all panels, the red bars denote AEMs and the blue bars denote CEMs. The error bars represent the propagated standard error of at least three replicates.

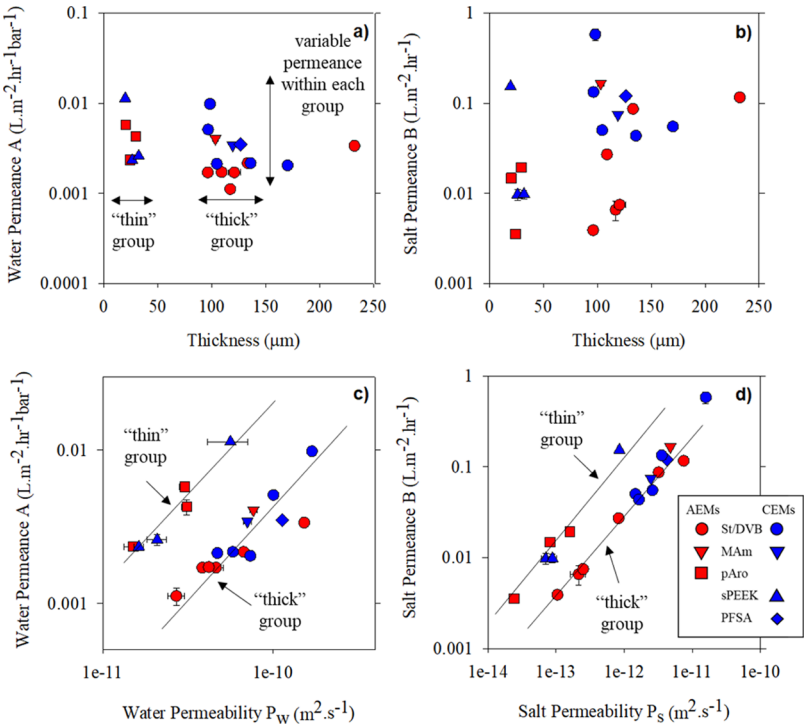

Figure 4. Water and salt permeance of 20 commercial IEMs measured in 4 M NaCl and pure water vs membrane thickness L (a,b) and permeability P (c,d). The lines in panels (c,d) are drawn to guide the eye. The red symbols denote AEMs, the blue symbols denote CEMs, and the shape of the symbol indicates the membrane polymer type [see legend in the inset of panel (d)]. The error bars represent the propagated standard error of at least three replicates. Refer to Table 1 for definitions of the membrane polymer abbreviations.

4. RESULTS AND DISCUSSION

4.1. Membrane Permeance. *4.1.1. Water Permeance.* We first consider the water permeance of 20 commercial IEMs. Water permeance varied over about 1 order of magnitude among the IEMs tested, from 0.001 to 0.011 L m^{-2} h^{-1} bar^{-1} (Figure 3a,b, solid bars, Table S3), consistent with the range of values reported in the literature (0.005−0.17 L m^{-2} h^{-1} bar^{-1}).[13,22,24,25] It is noteworthy that the water permeance of CEMs was generally higher than that of the AEMs.

4.1.2. Salt Permeance. The salt permeance of the IEMs varied by ∼2.5 orders of magnitude, from 0.002 to 0.5 L m^{-2} h^{-1} (Figure 3a,b, empty bars, Table S3). This range of values is consistent with data reported by Porada et al.[20] for lab-prepared IEMs based on FAS and FKE polymer solutions (0.003−0.025 L m^{-2} h^{-1}). Similar to the results for water permeance, CEMs generally had higher salt permeance than AEMs, but the contrast between CEMs and AEMs was greater than that seen for water permeance.

4.2. Contribution of Water and Salt Permeability to Permeance. Having observed variations of several orders of magnitude in both the water and salt permeance of IEMs, we next sought to understand whether those variations were caused by differences in material properties (i.e., permeability) or geometry (i.e., thickness). Thus, we will now discuss measured water and salt permeability, membrane thickness, and their relationship with permeance.

4.2.1. Water Permeability. Water permeance is related to water permeability P_w according to[10,42]

$$A = \frac{P_w}{L}\frac{V_w}{RT} \tag{16}$$

According to eq 16, variations in P_w and L together comprise all of the variation in A by definition. Thus, by examining the

DOI: 10.1021/acsami.8b14494
ACS Appl. Mater. Interfaces 2018, 10, 39745−39756

magnitudes of the respective variations in P_w and L, we can gain insight into which of the two variables makes a greater contribution to variations in permeance. Note that eq 16 is approximate in the case of highly swollen polymers[10,42] such as some of our IEMs. We present it here for the purpose of discussion, as we obtain the same conclusion when using a more rigorous equation (see Supporting Information).

Figure 4a presents a plot of water permeance versus thickness for all IEMs studied. The thicknesses of the membranes varied by approximately 1 order of magnitude, from 20 to 232 μm (Table 1). The thickness values clustered into roughly two groups along the x-axis: a "thin" group (20−32 μm) and a "thick" group (96−136 μm, Figure 4a and Table 1). With the exception of Nafion (N115), all nonreinforced IEMs were in the "thin" group, whereas all reinforced IEMs were in the "thick" group. Inspection of Figure 4a shows that within each thickness group, A varied by nearly an order of magnitude. Thus, there were substantial differences in water permeance among IEMs with approximately the same thickness, indicating that variations in water permeance were driven primarily by differences in permeability. Furthermore, a plot of log A versus log P_w (Figure 4c) shows that higher permeance was closely associated with higher permeability within each thickness group. As with permeance, the permeability within each thickness group varied over nearly an order of magnitude from $\sim 2 \times 10^{-11}$ to 2×10^{-10} m^2 s^{-1} (Figures 4c and S2), reinforcing the conclusion that variations in permeance were driven by variations in permeability rather than in thickness.

4.2.2. Salt Permeability. As was the case with water, the salt permeability and thickness determine salt permeance by definition (see eq 15). Figure 4b presents salt permeance versus thickness and shows that the permeance within each of the thickness groups varied by roughly 2 orders of magnitude. Thus, we can conclude that differences in salt permeance were primarily attributable to differences in salt permeability rather than differences in thickness. The salt permeability varied over $\sim$3 orders of magnitude across all membranes, from 10^{-11} to 10^{-14} m^2 s^{-1} (Figure 4d), consistent with the range of 10^{-11} to 10^{-12} m^2 s^{-1} reported by Berezina et al. for a range of commercial IEMs.[23,49] Similar to water, higher salt permeance was clearly associated with higher permeability within each thickness group (Figures 4d and S2).

In summary, we found that the substantial (1−3 order of magnitude) differences in water and salt permeance among IEMs were primarily attributable to differences in the respective permeabilities of the membranes, rather than differences in their thickness.

4.3. Contribution of Partitioning and Diffusivity to Permeability. Because we observed substantial variations in permeability among IEMs and those variations were the primary factor affecting membrane permeance, we will now examine the partition and diffusion coefficients of the IEMs, which together determine the permeability (see eq 1).

4.3.1. Water Partition and Diffusion Coefficients. We first consider the partition and diffusion coefficients of water in the IEMs (Figure 5a,c, Tables S3 and S4). The water partition coefficient K_w varied from 0.1 to 0.35, while the water diffusion coefficient D_w varied by about 1 order of magnitude, from 10^{-10} to 10^{-9} m^2 s^{-1}. The obtained values of D_w were consistent with average D_w values for six commercial IEM pairs reported by Veerman et al.[11] (5.8×10^{-11} to 7.9×10^{-9} m^2 s^{-1}). K_w is not usually reported for IEMs, but the corresponding SDs (0.09−0.37, Table 1) are in the same range as those reported by Güler et al.[4] for 12 commercial IEMs (0.08−0.56). Ji et al.[50] reported K_w = 0.06−0.51 in a series of lab-synthesized CEMs, which is also similar to the range we obtained. The fact that D_w varied over a substantially larger range than K_w ($\sim$10× vs $\sim$3×) indicates that variations in D_w were more important than variations in K_w in explaining variations in P_w. Furthermore, although neither D_w nor K_w clustered into groups as thickness did, we observed that for any given value of K_w, D_w varied by up to 1 order of magnitude (Figure S3). In contrast, for any given value of D_w, K_w varied over a substantially smaller range.

D_w and K_w were not correlated with each other ($R^2 < 0.02$, $p = 0.41$, Figure S3). This lack of correlation indicates that water partitioning (water sorption) is not strongly coupled to the rate of water transport in IEMs. This finding suggests that water molecules hydrating the fixed charge sites within the polymer are relatively immobile. That is, a highly charged IEM may absorb a great deal of water (high K_w) but only "free" water molecules within the structure contribute to diffusion (thus high K_w does not necessarily lead to high D_w).

4.3.2. Salt Partition and Diffusion Coefficients. The salt partition coefficients K_s ranged from 0.05 to 0.24 (Figure 5b, Tables S4 and S5), while the salt diffusion coefficients D_s varied from about 10^{-10} to 10^{-13} m^2 s^{-1} (Figure 5b, Tables S4 and S5). The obtained values of K_s were similar to the range reported by Kamcev et al.[9] for three commercial IEMs in 1 M sodium chloride (0.08−0.14) and to values for several lab-synthesized CEMs in 0.5 or 1 M sodium chloride reported in other studies[50,51] (0.2−0.25). D_s values also compared well with previous reports in the literature (1.8×10^{-14} to 1×10^{-10} m^2 s^{-1}).[11,52−54] The larger variation in D_s compared to D_w (3 orders of magnitude vs 1 order of magnitude, respectively) was consistent with previous reports as well; Veerman et al.[11] reported that D_s ranged from 1.8×10^{-14} to 3.2×10^{-11} m^2 s^{-1}, while D_w ranged from 5.8×10^{-11} to 7.9×10^{-9} m^2 s^{-1} for a set of commercial IEM pairs.

As was the case with water, D_s varied over a substantially larger range than K_s. For any given value of K_s, D_s varied by at least 1 order of magnitude (Figure S3). The much larger variation in D_s compared to K_s (1000× vs 5×) indicates that diffusion was primarily responsible for the observed variations in P_s among IEMs. Both log D_s and K_s correlated strongly with log P_s ($p < 0.01$, Figure 5b,d), but similar to water, the regression coefficient for the diffusion coefficient was greater than that for the partition coefficient (R^2 = 0.96 vs 0.56, respectively), reinforcing the conclusion that variations in D_s drive variations in P_s.

D_s and K_s were weakly correlated with one another (R^2 = 0.36, $p < 0.01$, Figure S3), indicating that partitioning and diffusion of mobile salt in IEMs are coupled to some extent. This is in contrast to the finding for water that diffusion and partitioning were not correlated (Figure S3).

In summary, for both water and salt, permeability was correlated with diffusion and partition coefficients. However in both cases, P and D varied over several orders of magnitude, whereas K varied over a much smaller range, indicating that differences in diffusion coefficient were the primary cause of variations in permeability. D_w and K_w were not correlated, whereas D_s and K_s were weakly correlated.

4.4. Membrane Polymer Type. Having examined the water and salt transport properties of commercial IEMs in aggregate, we will now consider differences in transport

DOI: 10.1021/acsami.8b14494
ACS Appl. Mater. Interfaces 2018, 10, 39745−39756

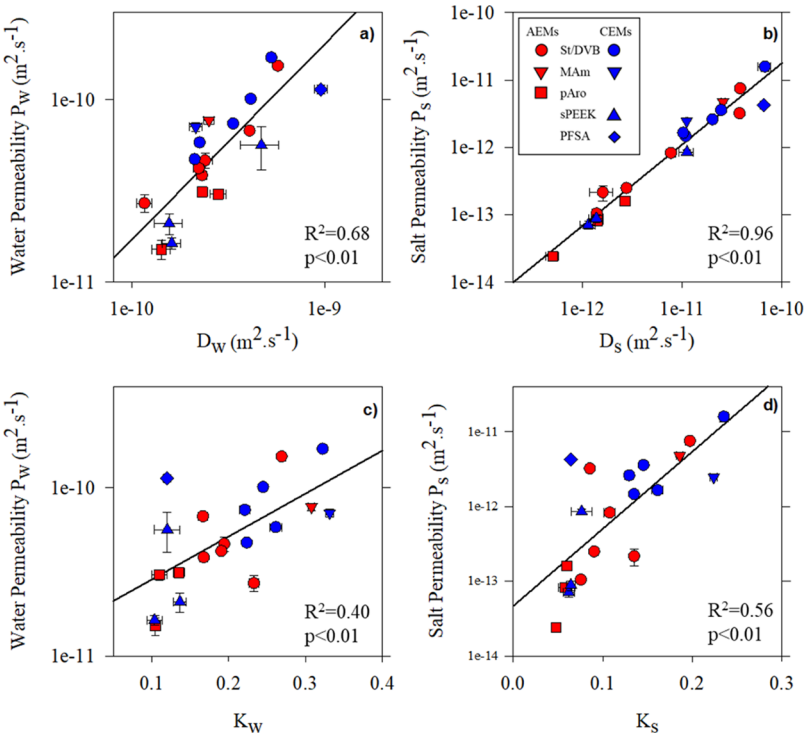

Figure 5. Water and salt transport properties of 20 commercial IEMs measured in a diffusion cell containing 4 M NaCl and pure water. (a) Water permeability vs water diffusion coefficient. (b) Salt permeability vs salt diffusion coefficient. (c) Water permeability vs water partition coefficient. (d) Salt permeability vs salt partition coefficient. The red symbols denote AEMs, the blue symbols denote CEMs, and the shape of the symbol indicates the membrane polymer type [see legend in the inset of panel (b)]. The error bars represent the propagated standard error of at least three replicates. Refer to Table 1 for definitions of the membrane polymer abbreviations.

properties among different membrane polymers. It is evident from Figure 4c,d that membranes in the "thick" group generally had higher permeability than those in the "thin" group (although the ranges overlap). This finding is surprising, considering that all of the membranes in the "thick" group except for one are reinforced, whereas all "thin" membranes lack reinforcement. Galizia et al. found that the presence of reinforcing material lowered the measured permeability of commercial IEMs by making ion diffusion pathways more tortuous.[31] Therefore, the true permeability of active polymers comprising the "thick" membranes is even higher than that indicated in Figure 4. The fact that membranes with higher permeability are thicker may be explained by considering that these IEMs are engineered for commercial applications: manufacturers may have sought to control permeance by increasing the thickness of the materials with higher permeability. However, it also reflects differences in behavior among different polymers (different symbol shapes in Figures 4–7). The "thin" group consisted only of pAro and sPEEK-based IEMs (squares and upward-facing triangles, respectively), while the "thick" group included the St/DVB-, PFSA-, and MaM-based IEMs (circles, diamond, and downward-facing triangles, respectively). Thus, the apparent trend of increasing permeability with increasing thickness may simply reflect the differences in permeability between these two classes of materials.

Comparing these two membrane groups in more detail shows that in general, the pAro- and sPEEK-based IEMs had lower permeabilities than the other IEMs (Figure 4c,d). The average P_w and P_s of the "thin" IEMs were 37% and just 6%, respectively, of the corresponding values for the "thick" IEMs. We observed a similar trend for partitioning, in which the

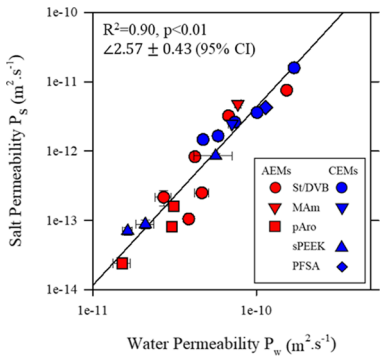

Figure 6. Water and salt permeability of 20 commercial IEMs measured in a diffusion cell containing 4 M sodium chloride solution and pure water. The red symbols denote AEMs, the blue symbols denote CEMs, and the shape of the symbol indicates the membrane polymer type (see legend). The error bars represent the propagated standard error of at least three replicates. Refer to Table 1 for definitions of the membrane polymer abbreviations.

"thin" IEMs on average had lower K_w and K_s (approximately 50% of the value for "thick" IEMs, Figure 5c,d). By contrast, there was little apparent difference in D_w among the groups (Figure 5a). For D_s, five of the six IEMs in the "thin" group had D_s values approximately 1 order of magnitude lower than the other IEMs, with the exception of three monovalent-selective AEMs from the "thick" group (three red circles at the lower left of Figures 4d or 5b). As a result, the average D_s for the "thin" group was only 13% of the average value for the other membranes. Consistent with the finding in Section 4.3 that differences in the diffusion coefficient are the primary cause of

DOI: 10.1021/acsami.8b14494
ACS Appl. Mater. Interfaces 2018, 10, 39745–39756

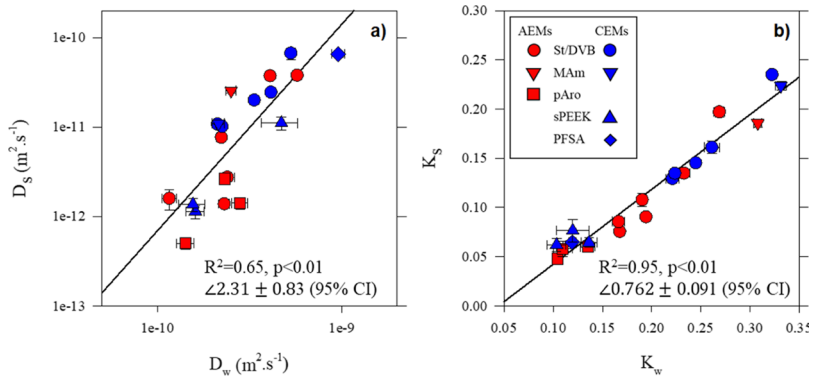

Figure 7. Water and salt (a) diffusion coefficients and (b) partition coefficients of 20 commercial IEMs measured in a diffusion cell containing 4 M sodium chloride solution and pure water. The red symbols denote AEMs, the blue symbols denote CEMs, and the shape of the symbol indicates the general polymer making up the membrane [see legend in the inset of panel (b)]. The error bars represent the propagated standard error of at least three replicates. Refer to Table 1 for definitions of the membrane polymer abbreviations.

variations in permeability, the lower D_s of the "thin" group of membranes explains why the "thin" IEMs have a substantially lower salt permeability than the others. The substantially lower D_s values of the monovalent-selective AEMs within the "thick" group can be explained by the presence of heavily cross-linked coatings on these membranes that impart additional hindrance to ion transport.[55,56] The fact that the AEMs with coatings made from a completely different material had D_s values similar to the IEMs in the "thin" group suggests that steric effects may explain differences in performance between the groups.

Overall, the pAro- and sPEEK-based IEMs had somewhat lower P, D, and K values than the other IEMs, but the ranges for most parameters overlapped with those of IEMs based on other materials. Thus, not surprisingly, differences in the membrane polymer type influence water and salt transport. However, the overlap between polymer types and the significant range of variation in most transport properties among IEMs made of the same polymer type indicate that other factors play a larger role in modulating water and salt transport. For example, the large variation in properties among membranes based on St/DVB chemistry (which are produced by several different manufacturers) could reflect differences in the reinforcing material used in these membranes.

4.5. Relationships between Water and Salt Transport. To further explore the factors that govern transport properties, we next consider relationships between water and salt transport. Figure 6 shows that log P_w and log P_s were strongly correlated for all IEMs studied (R^2 = 0.90, p < 0.01). Remarkably, all IEMs fell on the same trend line, irrespective of the polymer backbone, reinforcing, or charge (positively charged AEM or negatively charged CEM). Both AEMs and CEMs span the entire range of P_w and P_s, and most individual membrane polymers span a significant range as well. Yet for all membranes, higher water permeability was associated with higher salt permeability. This striking result provides evidence that in highly swollen polymers like IEMs, unassociated cations and anions (i.e., mobile salt) do not have significant interactions with the polymer chains because of the large amount of free volume available for permeation.[57] If such interactions were significant, we would expect different membrane polymers to have different relative rates of water and salt transport, because charged ions and neutral water would interact differently with each polymer. Our finding is qualitatively consistent with previous observations that the transport numbers of water and of counter-ions are linearly correlated to one another in commercial IEMs.[23]

The slope of the regression line in Figure 6 (2.57 ± 0.43) indicates that a unit change in water permeability is accompanied by a proportionally larger change in salt permeability. The larger change in P_s for a given change in P_w is consistent with free-volume theory, which states that the diffusion rate of a larger penetrant relative to a smaller one (i.e., salt relative to water) increases as the free-volume element size increases.[10,42,58] Therefore, salt permeability should be more sensitive than water permeability to changes in free volume (i.e., membrane microstructure).

We observed relationships between water and salt diffusion coefficients that generally paralleled those observed with permeability. log D_w and log D_s correlated moderately well (R^2 = 0.65, p < 0.01, Figure 7a), and the slope of the regression line (2.31) indicates that a unit change in water diffusivity is accompanied by a proportionally larger change in salt diffusivity. The correlation between water and salt diffusivity suggests that similar physical mechanisms (likely steric hindrance) underlie both water and salt diffusion through IEMs, while the proportionally higher change in D_s compared to D_w is consistent with free-volume theory as discussed above. The apparent importance of steric hindrance to the permeability and diffusion rates of water and salt indicates that water and salt transport in IEMs is controlled primarily by the membrane microstructure (e.g., pore size and connectivity) and reinforces the conclusion that chemical interactions with the polymer chain are limited in IEMs. In other words, the differences in P, D, and K that we observed among different materials can be attributed to differences in the microstructure.

Similar to permeabilities and diffusion coefficients, partition coefficients for water and salt also correlated very strongly (R^2 = 0.95, p < 0.01, Figure 7b), which can be rationalized with reference to fixed charge concentration. The membranes with lower water uptake (low K_w and correspondingly low SD, Table 1) tend to have higher fixed charge concentrations (see eq 7). Their high charge promotes strong Donnan exclusion of co-ions, reducing the quantity of mobile salt in the membrane and lowering K_s. Therefore, the membranes with low K_w tend to have low K_s and vice-versa.

DOI: 10.1021/acsami.8b14494
ACS Appl. Mater. Interfaces 2018, 10, 39745−39756

5. CONCLUSIONS

In this work, we measured the water and salt transport properties of 20 commercial ion exchange membranes (IEMs) and investigated relationships between water and salt transport properties and membrane polymer type. The following points summarize our main findings:

- Water and salt permeance varied over a wide range (1−3 orders of magnitude), even among membranes with similar thickness, suggesting that differences in permeability drive differences in permeance among commercial IEMs.
- Variations in diffusion coefficients among IEMs were the primary factors determining variations in permeability among membranes.
- Permeability, diffusion, and partition coefficients for water were highly correlated with those for salt. Strikingly, all IEMs fell on the same trendline, regardless of the membrane polymer, charge (AEM or CEM), or reinforcement. This result indicates that water and salt transport are determined primarily by the microstructure of the membrane rather than by the polymer chemistry or charge and provides clear evidence that ions do not interact strongly with polymer chains in highly swollen IEMs.

The above findings offer insights that inform advanced IEM development. As stated in the Introduction, it is desirable to develop IEMs that minimize salt diffusion and water transport to maximize the energy efficiency of electrochemical processes. We have shown that the membrane microstructure appears to be the primary factor controlling rates of water and salt transport in IEMs, rather than chemical interactions with the polymer chain. Recognition of this fact by the membrane research community may open new polymer chemistries and processing methods for consideration that have not previously been studied as ion-exchange materials. To facilitate the design of new membrane polymers, future studies should investigate which physicochemical properties best describe the variations in transport behavior we observed among materials.

■ ASSOCIATED CONTENT

Supporting Information

The Supporting Information is available free of charge on the ACS Publications website at DOI: 10.1021/acsami.8b14494.

Derivation of mass balance for simultaneous determination of water and salt permeability in a two-compartment cell; water permeability conversions in highly swollen polymers; example water and salt permeance data; estimated effect of the membrane reinforcing fabric on observed transport properties; method details for ICP−MS analysis of sodium; tabulated results for important parameters measured and calculated in this study; plots of permeability versus membrane thickness; plots of diffusion coefficient versus partition coefficient; comparison of measured IEC with literature and manufacturer-supplied data (PDF)

■ AUTHOR INFORMATION

Corresponding Author

*E-mail: coronell@unc.edu. Phone: 1-919-966-9010. Fax: +1-919-966-7911.

ORCID

R. S. Kingsbury: 0000-0002-7168-3967
S. Zhu: 0000-0001-5128-841X
O. Coronell: 0000-0002-7018-391X

Notes

The authors declare no competing financial interest.

■ ACKNOWLEDGMENTS

We wish to acknowledge Peter Cable at the UNC Biomarker Mass Spectrometry Facility for his assistance with ICP-MS analysis. This work was funded by the University of North Carolina Research Opportunities Initiative (ROI) program, the UNC Gillings Innovation Laboratories (GIL) Program, and the UNC Collaboratory. R.S.K. was supported by the National Science Foundation Graduate Research Fellowship Program under grant no. DGE-1144081. Any opinions, findings, and conclusions or recommendations expressed in this material are those of the authors and do not necessarily reflect the views of the National Science Foundation. A preprint version of this article is available on ChemRxiv.[59]

■ REFERENCES

(1) Aulick, R. *Progress Towards Commercialization of a Novel Low-Energy Desalination System*; Singapore International Water Week: Singapore, 2014.
(2) Fane, A. G.; Wang, R.; Hu, M. X. Synthetic Membranes for Water Purification: Status and Future. *Angew. Chem., Int. Ed.* **2015**, *54*, 3368−3386.
(3) Alvarez-Silva, O. A.; Osorio, A. F.; Winter, C. Practical Global Salinity Gradient Energy Potential. *Renewable Sustainable Energy Rev.* **2016**, *60*, 1387−1395.
(4) Güler, E.; Elizen, R.; Vermaas, D. A.; Saakes, M.; Nijmeijer, K. Performance-Determining Membrane Properties in Reverse Electrodialysis. *J. Membr. Sci.* **2013**, *446*, 266−276.
(5) Dlugolecki, P.; Nymeijer, K.; Metz, S.; Wessling, M. Current Status of Ion Exchange Membranes for Power Generation from Salinity Gradients. *J. Membr. Sci.* **2008**, *319*, 214−222.
(6) Hong, J. G.; Zhang, B.; Glabman, S.; Uzal, N.; Dou, X.; Zhang, H.; Wei, X.; Chen, Y. Potential ion exchange membranes and system performance in reverse electrodialysis for power generation: A review. *J. Membr. Sci.* **2015**, *486*, 71−88.
(7) Strathmann, H. *Introduction to Membrane Science and Technology*; Wiley-VCH Verlag: Weinheim, Germany, 2011.
(8) Kamcev, J.; Freeman, B. D. Charged Polymer Membranes for Environmental/Energy Applications. *Annu. Rev. Chem. Biomol. Eng.* **2016**, *7*, 111−133.
(9) Kamcev, J.; Paul, D. R.; Manning, G. S.; Freeman, B. D. Predicting Salt Permeability Coefficients in Highly Swollen, Highly Charged Ion Exchange Membranes. *ACS Appl. Mater. Interfaces* **2017**, *9*, 4044−4056.
(10) Geise, G. M.; Paul, D. R.; Freeman, B. D. Fundamental Water and Salt Transport Properties of Polymeric Materials. *Prog. Polym. Sci.* **2014**, *39*, 1−42.
(11) Veerman, J.; de Jong, R. M.; Saakes, M.; Metz, S. J.; Harmsen, G. J. Reverse Electrodialysis: Comparison of Six Commercial Membrane Pairs on the Thermodynamic Efficiency and Power Density. *J. Membr. Sci.* **2009**, *343*, 7−15.
(12) Yip, N. Y.; Vermaas, D. A.; Nijmeijer, K.; Elimelech, M. Thermodynamic, Energy Efficiency, and Power Density Analysis of Reverse Electrodialysis Power Generation with Natural Salinity Gradients. *Environ. Sci. Technol.* **2014**, *48*, 4925−4936.
(13) Tedesco, M.; Hamelers, H. V. M.; Biesheuvel, P. M. Nernst-Planck Transport Theory for (Reverse) Electrodialysis: II. Effect of Water Transport through Ion-Exchange Membranes. *J. Membr. Sci.* **2017**, *531*, 172−182.

(14) Kingsbury, R. S.; Coronell, O. Osmotic Ballasts Enhance Faradaic Efficiency in Closed-Loop, Membrane-Based Energy Systems. *Environ. Sci. Technol.* **2017**, *51*, 1910−1917.
(15) Kingsbury, R. S.; Chu, K.; Coronell, O. Energy Storage by Reversible Electrodialysis: The Concentration Battery. *J. Membr. Sci.* **2015**, *495*, 502−516.
(16) Helfferich, F. *Ion Exchange*; McGraw-Hill: New York, 1962.
(17) Wijmans, J. G.; Baker, R. W. The Solution-Diffusion Model: A Review. *J. Membr. Sci.* **1995**, *107*, 1−21.
(18) Yip, N. Y.; Elimelech, M. Comparison of Energy Efficiency and Power Density in Pressure Retarded Osmosis and Reverse Electrodialysis. *Environ. Sci. Technol.* **2014**, *48*, 11002−11012.
(19) Tedesco, M.; Hamelers, H. V. M.; Biesheuvel, P. M. Nernst-Planck Transport Theory for (Reverse) Electrodialysis: I. Effect of Co-Ion Transport through the Membranes. *J. Membr. Sci.* **2016**, *510*, 370−381.
(20) Porada, S.; van Egmond, W. J.; Post, J. W.; Saakes, M.; Hamelers, H. V. M. Tailoring Ion Exchange Membranes to Enable Low Osmotic Water Transport and Energy Efficient Electrodialysis. *J. Membr. Sci.* **2018**, *552*, 22−30.
(21) van Egmond, W. J.; Starke, U. K.; Saakes, M.; Buisman, C. J. N.; Hamelers, H. V. M. Energy Efficiency of a Concentration Gradient Flow Battery at Elevated Temperatures. *J. Power Sources* **2017**, *340*, 71−79.
(22) van Egmond, W. J.; Saakes, M.; Porada, S.; Meuwissen, T.; Buisman, C. J. N.; Hamelers, H. V. M. The Concentration Gradient Flow Battery as Electricity Storage System: Technology Potential and Energy Dissipation. *J. Power Sources* **2016**, *325*, 129−139.
(23) Berezina, N. P.; Kononenko, N. A.; Dyomina, O. A.; Gnusin, N. P. Characterization of Ion-Exchange Membrane Materials: Properties vs Structure. *Adv. Colloid Interface Sci.* **2008**, *139*, 3−28.
(24) Bevacqua, M.; Carubia, A.; Cipollina, A.; Tamburini, A.; Tedesco, M.; Micale, G. Performance of a RED System with Ammonium Hydrogen Carbonate Solutions. *Desalin. Water Treat.* **2016**, *57*, 23007−23018.
(25) Evans, C. E.; Noble, R. D.; Nazeri-Thompson, S.; Nazeri, B.; Koval, C. A. Role of Conditioning on Water Uptake and Hydraulic Permeability of Nafion Membranes. *J. Membr. Sci.* **2006**, *279*, 521−528.
(26) Galama, A. H.; Post, J. W.; Hamelers, H. V. M.; Nikonenko, V. V.; Biesheuvel, P. M.; Leeuwarden, M. A. On the Origin of the Membrane Potential Arising across Densely Charged Ion Exchange Membranes: How Well Does the Teorell-Meyer-Sievers Theory Work? *J. Membr. Sci. Res.* **2015**, *2*, 128−140.
(27) Sata, T. *Ion Exchange Membranes: Preparation, Characterization, Modification, and Application*; Royal Society of Chemistry: Cambridge, 2004.
(28) Fujioka, T.; Oshima, N.; Suzuki, R.; Price, W. E.; Nghiem, L. D. Probing the Internal Structure of Reverse Osmosis Membranes by Positron Annihilation Spectroscopy: Gaining More Insight into the Transport of Water and Small Solutes. *J. Membr. Sci.* **2015**, *486*, 106−118.
(29) Kamcev, J.; Galizia, M.; Benedetti, F. M.; Jang, E.-S.; Paul, D. R.; Freeman, B. D.; Manning, G. S. Partitioning of Mobile Ions Between Ion Exchange Polymers and Aqueous Salt Solutions: Importance of Counter-Ion Condensation. *Phys. Chem. Chem. Phys.* **2016**, *18*, 6021−6031.
(30) Kamcev, J.; Paul, D. R.; Freeman, B. D. Ion Activity Coefficients in Ion Exchange Polymers: Applicability of Manning's Counterion Condensation Theory. *Macromolecules* **2015**, *48*, 8011−8024.
(31) Galizia, M.; Benedetti, F. M.; Paul, D. R.; Freeman, B. D. Monovalent and divalent ion sorption in a cation exchange membrane based on cross-linked poly (p-styrene sulfonate-co-divinylbenzene). *J. Membr. Sci.* **2017**, *535*, 132−142.
(32) Van Berchum, B.; Van Baak, W. J.; Hessing, J. Curable Composition and Membranes. U.S. Patent 20,140,378,561 A1, 2014.
(33) Takamoto, T.; Amao, A.; Yamada, W. Functional Polymer Membrane and Method of Producing the Same. U.S. Patent 9,441,083 B2, 2016.
(34) Geise, G. M.; Cassady, H. J.; Paul, D. R.; Logan, B. E.; Hickner, M. A. Specific Ion Effects on Membrane Potential and the Permselectivity of Ion Exchange Membranes. *Phys. Chem. Chem. Phys.* **2014**, *16*, 21673−21681.
(35) Geise, G. M.; Hickner, M. A.; Logan, B. E. Ionic Resistance and Permselectivity Tradeoffs in Anion Exchange Membranes. *ACS Appl. Mater. Interfaces* **2013**, *5*, 10294−10301.
(36) Tanaka, Y. Fundamental Properties of Ion Exchange Membranes. *Ion Exchange Membranes: Fundamentals and Application*, Elsevier, 2015; pp 29−65.
(37) Wypych, G.; Wypych, G. PEEK Polyetheretherketone. *Handbook of Polymers*, 2012; pp 353−358.
(38) Wypych, G.; Wypych, G. PTFE Polytetrafluoroethylene. *Handbook of Polymers*, 2012; pp 566−570.
(39) Wypych, G.; Wypych, G. PPO Poly(Phenylene Oxide). *Handbook of Polymers*, 2012; pp 504−507.
(40) Wypych, G.; Wypych, G. PS Polystyrene. *Handbook of Polymers*, 2012; pp 541−547.
(41) Insurance, I. for O. S. and H. of the G. S. A. Methacrylamide. http://www.dguv.de/ifa/gestis/gestis-stoffdatenbank/index-2.jsp (accessed Nov 29, 2017).
(42) Zhang, H.; Geise, G. M. Modeling the Water Permeability and Water/Salt Selectivity Tradeoff in Polymer Membranes. *J. Membr. Sci.* **2016**, *520*, 790−800.
(43) Kamcev, J.; Jang, E.-S.; Yan, N.; Paul, D. R.; Freeman, B. D. Effect of Ambient Carbon Dioxide on Salt Permeability and Sorption Measurements in Ion-Exchange Membranes. *J. Membr. Sci.* **2015**, *479*, 55−66.
(44) Varcoe, J. R.; Atanassov, P.; Dekel, D. R.; Herring, A. M.; Hickner, M. A.; Kohl, P. A.; Kucernak, A. R.; Mustain, W. E.; Nijmeijer, K.; Scott, K.; Xu, T.; Zhuang, L. Anion-Exchange Membranes in Electrochemical Energy Systems. *Energy Environ. Sci.* **2014**, *7*, 3135−3191.
(45) Kamcev, J.; Paul, D. R.; Freeman, B. D. Effect of Fixed Charge Group Concentration on Equilibrium Ion Sorption in Ion Exchange Membranes. *J. Mater. Chem. A* **2017**, *5*, 4638−4650.
(46) Pitzer, K. S.; Peiper, J. C.; Busey, R. H. Thermodynamic Properties of Aqueous Sodium Chloride Solutions. *J. Phys. Chem. Ref. Data* **1984**, *13*, 1−102.
(47) Pitzer, K. S.; Mayorga, G. Thermodynamics of electrolytes. II. Activity and osmotic coefficients for strong electrolytes with one or both ions univalent. *J. Phys. Chem.* **1973**, *77*, 2300−2308.
(48) May, P. M.; Rowland, D.; Hefter, G.; Königsberger, E. A Generic and Updatable Pitzer Characterization of Aqueous Binary Electrolyte Solutions at 1 bar and 25 °C. *J. Chem. Eng. Data* **2011**, *56*, 5066−5077.
(49) Gnusin, N. P.; Berezina, N. P.; Kononenko, N. A.; Dyomina, O. A. Transport Structural Parameters to Characterize Ion Exchange Membranes. *J. Membr. Sci.* **2004**, *243*, 301−310.
(50) Ji, Y.; Luo, H.; Geise, G. M. Specific Co-Ion Sorption and Diffusion Properties Influence Membrane Permselectivity. *J. Membr. Sci.* **2018**, *563*, 492−504.
(51) Yan, N.; Paul, D. R.; Freeman, B. D. Water and Ion Sorption in a Series of Cross-Linked AMPS/PEGDA Hydrogel Membranes. *Polymer* **2018**, *146*, 196−208.
(52) Hassanvand, A.; Chen, G. Q.; Webley, P. A.; Kentish, S. E. Improvement of MCDI Operation and Design through Experiment and Modelling: Regeneration with Brine and Optimum Residence Time. *Desalination* **2017**, *417*, 36−51.
(53) Miyoshi, H. Diffusion Coefficients of Ions through Ion-Exchange Membranes for Donnan Dialysis Using Ions of the Same Valence. *Chem. Eng. Sci.* **1997**, *52*, 1087−1096.
(54) Agarwal, C.; Chaudhury, S.; Pandey, A. K.; Goswami, A. Kinetic Aspects of Donnan Dialysis through Nafion-117 Membrane. *J. Membr. Sci.* **2012**, *415−416*, 681−685.

DOI: 10.1021/acsami.8b14494
ACS Appl. Mater. Interfaces 2018, 10, 39745−39756

(55) Vermaas, D. A.; Veerman, J.; Saakes, M.; Nijmeijer, K. Influence of Multivalent Ions on Renewable Energy Generation in Reverse Electrodialysis. *Energy Environ. Sci.* **2014**, *7*, 1434−1445.
(56) Güler, E.; van Baak, W.; Saakes, M.; Nijmeijer, K. Monovalent-Ion-Selective Membranes for Reverse Electrodialysis. *J. Membr. Sci.* **2014**, *455*, 254−270.
(57) Chang, K.; Xue, T.; Geise, G. M. Increasing Salt Size Selectivity in Low Water Content Polymers via Polymer Backbone Dynamics. *J. Membr. Sci.* **2018**, *552*, 43−50.
(58) Xie, W.; Ju, H.; Geise, G. M.; Freeman, B. D.; Mardel, J. I.; Hill, A. J.; McGrath, J. E. Effect of Free Volume on Water and Salt Transport Properties in Directly Copolymerized Disulfonated Poly(arylene ether sulfone) Random Copolymers. *Macromolecules* **2011**, *44*, 4428−4438.
(59) Kingsbury, R.; Zhu, S.; Flotron, S.; Coronell, O. Microstructure Determines Water and Salt Permeation in Commercial Ion Exchange Membranes. *ChemRxiv* **2018**, 1−36.

DOI: 10.1021/acsami.8b14494
ACS Appl. Mater. Interfaces 2018, 10, 39745−39756